BIOCHEMISTRY
including biophysical chemistry & molecular biology

Article

pubs.acs.org/biochemistry

Characterization of Variants of the Pore-Forming Toxin ClyA from *Escherichia coli* Controlled by a Redox Switch

Daniel Roderer,[†] Stephan Benke,[‡] Marcus Müller,[†,§] Helene Fäh-Rechsteiner,[†] Nenad Ban,[†] Benjamin Schuler,[‡] and Rudi Glockshuber*[,†]

[†]Institute of Molecular Biology and Biophysics, ETH Zürich, Otto-Stern-Weg 5, CH-8093 Zürich, Switzerland

[‡]Department of Biochemistry, University of Zurich, Winterthurerstrasse 190, CH-8057 Zurich, Switzerland

Supporting Information

ABSTRACT: The α-pore-forming toxin Cytolysin A (ClyA) is responsible for the hemolytic phenotype of several *Escherichia coli* and *Salmonella enterica* strains. ClyA is a soluble, 34 kDa monomer that assembles into a dodecameric pore complex in the presence of membranes or detergent. The comparison of the X-ray structures of monomeric ClyA and the ClyA protomer in the pore complex revealed one of the largest conformational transitions observed so far in proteins, involving the structural rearrangement of more than half of all residues, which is consistent with the finding that conversion from the monomer to the assembly competent protomer is rate-limiting for pore assembly. Here, we introduced artificial disulfide bonds at two distinct sites into the ClyA monomer that both prevent a specific structural rearrangement required for protomer formation. Using electron microscopy and hemolytic activity assays, we show that the engineered disulfides indeed trap these ClyA variants in an assembly incompetent state. Assembly of the variants into functional pore complexes can be completely recovered by disulfide reduction. The assembly kinetics of the ClyA variants recorded with circular dichroism and fluorescence spectroscopy revealed the same mechanism of protomer formation that was observed for wild-type ClyA, proceeding via an intermediate with decreased secondary structure content.

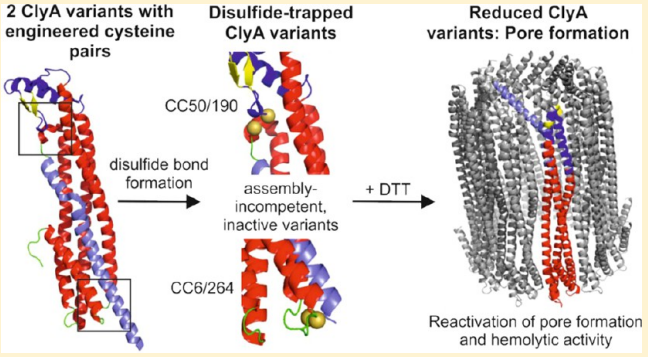

Pore-forming toxins (PFTs) are virulence factors of many bacterial and eukaryotic pathogens that kill target cells by inserting pores into the plasma membrane that cause cell lysis. PFTs can be classified according to their transmembrane segments.[1,2] While α-PFTs like diphtheria toxin[3] penetrate target membranes via transmembrane helices, β-PFTs like staphylococcal α-hemolysin[4] insert into membranes by forming β-barrels. A common feature of both α- and β-PFTs is their conversion from a soluble, monomeric state to a membrane-embedded, oligomeric pore complex. Membrane insertion and assembly of PFTs into active pore complexes are often accompanied by significant structural rearrangements.[5−8]

Cytolysin A (ClyA, also termed HlyE or SheA; 34 kDa per monomer) is a member of the α-PFT family and responsible for the hemolytic phenotype of various pathogenic *Escherichia coli* and *Salmonella enterica* strains.[9−11] In nonpathogenic *E. coli* strains, the transcription of *clyA* is repressed by the nucleotide binding protein H-NS,[12] which can be reversed by the regulatory protein SlyA.[13,14] Besides its hemolytic activity, ClyA can also kill cultured macrophages[15,16] and even lyse tumor cells.[17] ClyA is secreted into the extracellular medium as an annular, homo-oligomeric pore complex in outer membrane vesicles (OMVs).[18] The mechanism of translocation of ClyA from the cytosol to OMVs is still poorly understood. ClyA does not possess a cleavable, N-terminal signal sequence for periplasmic secretion, but its N- and C-terminal α-helical segments, together with a flanking hydrophobic patch, are required for translocation of ClyA through the cytoplasmic membrane.[19] ClyA can also be used as the N- or C-terminal fusion tag to secrete other proteins via OMVs.[20]

The soluble ClyA monomer (Figure 1A) is composed of two domains: (i) a large tail domain (residues 1−159 and 206−303) consisting of a bundle of one short α-helix and four long α-helices and (ii) a small head domain (residues 160−205) composed of two short α-helices flanking a hydrophobic β-hairpin element termed the β-tongue.[5,21] Because of the hydrophobic character of the β-tongue region, it is supposed to be the first part of ClyA that inserts into target membranes, and introduction of charged residues into the β-tongue or a deletion from the β-tongue leads to a strongly decreased membrane permeation activity.[19,22]

Assembly of ClyA into ring-shaped, dodecameric, pore complexes can be triggered *in vitro* by addition of membranes or detergents.[23] We recently determined the three-dimensional structure of the intact, dodecameric ClyA pore complex.[5] The

Received: June 17, 2014
Revised: September 12, 2014
Published: September 15, 2014

dx.doi.org/10.1021/bi5007578 | *Biochemistry* 2014, 53, 6357−6369

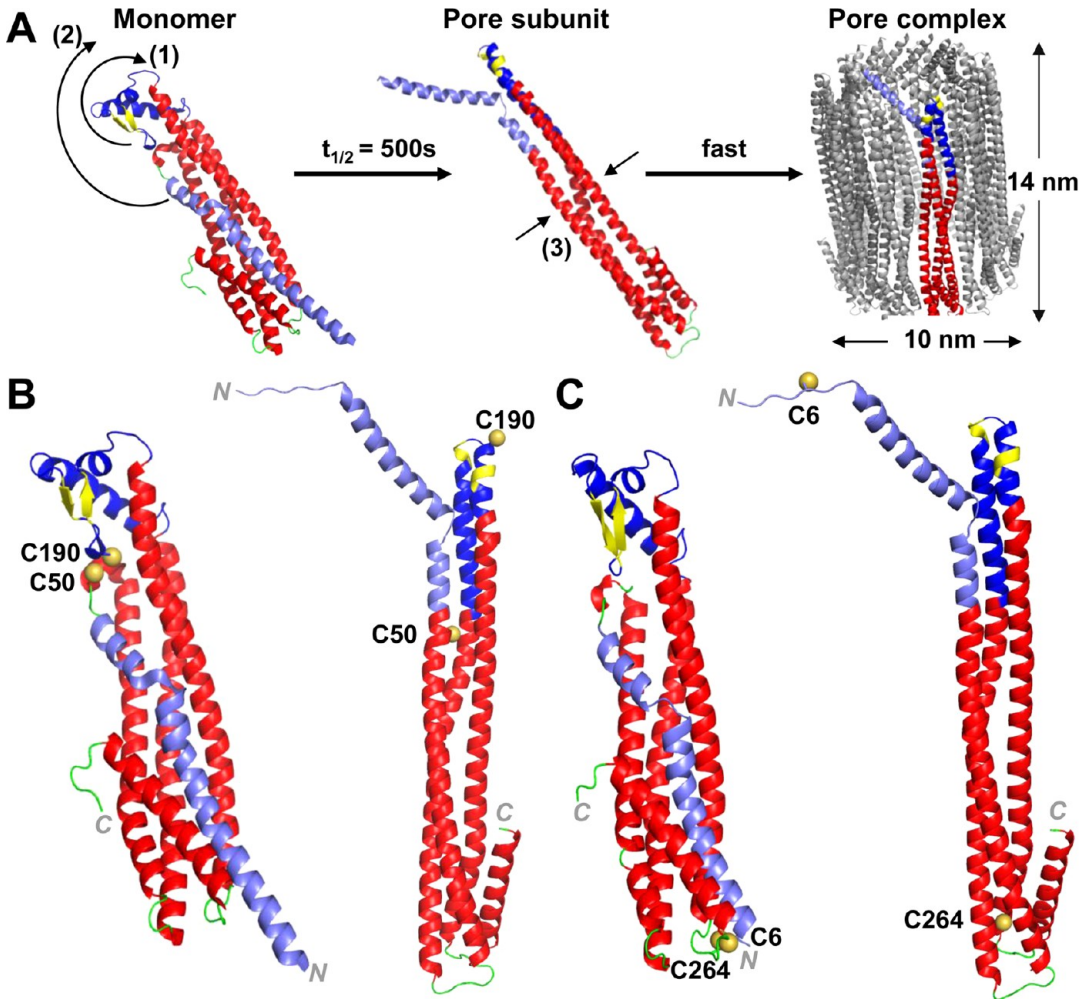

Figure 1. ClyA assembly mechanism and positions of engineered cysteines in the ClyA monomer (PDB entry 1QOY) and the pore subunit (PDB entry 2WCD). (A) Model of the conformational transition of ClyA from the soluble monomer to the dodecameric pore complex. Binding of the hydrophobic β-tongue (yellow) in the head domain (blue) to the target membrane may trigger the rearrangement of the head domain and elongate the neighboring helices (1). This may be followed by a swing-up movement of the N-terminal helix (light blue) (2) and a rearrangement of the remaining helices (3) in the tail domain (red) that form the intersubunit interface. At pH 7.3, 22 °C, and ClyA monomer concentrations in the μM range, the rate-limiting step of detergent (DDM)-induced pore assembly is the formation of the assembly competent protomer ($t_{1/2}$ = 500 s), which is followed by fast oligomerization of the subunits to the dodecameric pore. (B) Positions of the engineered cysteines at residues 50 and 190 for immobilizing the β-tongue with a disulfide bond. Models based on the structures of the ClyA monomer and one protomer in the pore complex are shown. (C) Position of the engineered disulfide bond between residues 6 and 264 that immobilizes the N-terminal ClyA helix in the 2.12 Å crystal structure of the CC6/264 monomer (left) and modeled position of Cys6 and Cys264 in the reduced protomer. Residues 2−7 are not resolved in the crystal structure of the pore complex and were modeled to visualize the position of Cys6. All figures were prepared with PyMol.[29]

comparison with the structure of the ClyA monomer revealed one of the largest conformational transitions observed so far in proteins involving the structural rearrangement of more than 50% of all ClyA residues (Figure 1A). The structural data agree with the observation that the unimolecular reaction from the monomer to the assembly competent protomer is the rate-limiting step in detergent-induced pore complex assembly *in vitro* at monomer concentrations in the range of 2.5−10 μM[23] (ClyA concentrations at which protomer assembly becomes rate-limiting have not yet been established). The monomer-to-protomer transition involves a series of structural rearrangements, including (i) the rearrangement of the head domain and the elongation of its neighboring α-helices, (ii) the swing-up movement of the N-terminal α-helix toward the membrane, and (iii) a structural rearrangement of the remaining helices of the tail region to an elongated four-helix bundle (Figure 1A). In the assembled, dodecameric pore complex, the N-terminal segments of the protomers (residues 1−34) penetrate the lipid bilayer and form a channel with an inner diameter of 3.5 nm[5] (Figure 1A).

To obtain further insight into the mechanism of ClyA assembly, we introduced artificial disulfide bonds that prevent the transition to the protomer at particular steps of the proposed conformational transition: (i) the structural rearrangement of the β-tongue region and (ii) the upward swing of the N-terminal α-helix (Figure 1B,C). We demonstrate that the disulfide bonds engineered to prevent these steps inhibit the transition of ClyA to assembly competent protomers. In contrast to previous reports on disulfide variants of the β-PFTs cholesterol-dependent cytolysin[24] and staphylococcal α-hemolysin[25] and the α-PFTs colicin A[26] and equinatoxin,[27] the engineered disulfides in ClyA completely block the assembly of pore complexes in the presence of membranes or detergent and trap ClyA in monomeric intermediate states with increased hydrophobicity. In addition, we show that the disulfide-trapped monomers can be reactivated

dx.doi.org/10.1021/bi5007578 | *Biochemistry* 2014, 53, 6357−6369

completely by reduction with dithiothreitol (DTT) to form active membrane pore complexes, demonstrating their potential for future technical applications.

MATERIALS AND METHODS

Materials. Chemicals of the highest available purity were purchased from Merck or Sigma-Aldrich. EDTA, glycerol, β-mercaptoethanol, and dithiothreitol (DTT) were obtained from AppliChem. *N*-Dodecyl β-D-maltopyranoside (DDM) was purchased from Anatrace, and horse erythrocytes were obtained from Oxoid AG. The fluorescent dyes Alexa Fluor 488 C_5-maleimide and Alexa Fluor 594 C_5-maleimide were purchased from Invitrogen.

Design and Cloning of *clyA* Variants. Using "Disulfide by Design",[28] we first analyzed the structure of the ClyA monomer for residues in the region of helix A and the β-tongue, i.e., the polypeptide segments undergoing the largest structural rearrangements upon protomer formation, which (i) can be connected with an artificial disulfide bond without major structural rearrangements in the monomer and (ii) are distant in the structure of the protomer. For the fixation of helix A, "Disulfide by Design"[28] predicted variants CC6/264 and CC17/277. While variant CC6/264 could be obtained in high yields (see below), variant CC17/277 (in which helix A would be connected to helix F) proved to be highly aggregation prone and was not further investigated. "Disulfide by Design"[28] did not identify potential residue pairs for fixing the β-tongue region with a disulfide bond. The β-tongue fixing variant CC50/190 was identified by modeling with PyMOL.[29]

Variants of the *clyA* gene with a single codon substitution were produced by QuikChange polymerase chain reaction (PCR)[30] in the context of the previously reported T7 expression plasmid (pET11a derivative) for wild-type (wt) *clyA* with an N-terminal His_6 tag.[23] Simultaneous replacement of the two natural Cys residues 87 and 285 with Ala yielded the cysteine-free ClyA pseudo-wild type, wt*, which was used as a template for the construction of redox-regulated variants with artificial disulfide bonds. Substitution of both Ala6 and Val264 codons with Cys codons then yielded variant CC6/264. Substitution of the Phe50 and Phe190 codons with Cys codons yielded variant CC50/190. For ClyA CC6/264, two further variants were constructed with cleavable, N-terminal His_6 tags. For this purpose, the cleavage sequence (ENLYFQ↓, with the arrow indicating the cleavage site) of TEV protease[31] was introduced between the sequence of the His_6 tag and the codons for Thr2 and Cys6, respectively. For cysteine-specific labeling of variant ClyA CC6/264 with donor/acceptor fluorophores, two additional cysteines were introduced into ClyA CC6/264 by QuikChange PCR (amino acid replacements Q56C and E252C, resulting in variant CC6/264 Q56C E252C).

Expression and Purification of ClyA Variants. ClyA variants were expressed and purified as described previously,[23] the only exception being that all purification steps were performed under reducing conditions in the presence of 2 mM β-mercaptoethanol (nickel chelate affinity chromatography) or 2 mM DTT (hydroxyapatite column). Protein production was conducted at 20 °C for 12 h. Proteins were purified by nickel chelate affinity chromatography followed by chromatography on hydroxyapatite as described previously.[23] The identity of all variants was confirmed by electrospray mass spectrometry. The concentration of ClyA and its variants was determined via their specific absorbance at 280 nm of 30370 M^{-1} cm^{-1}. Purification yields per liter of *E. coli* culture were 80, 27, 30, and 11 mg for ClyA wt, wt*, CC6/264, and CC50/190, respectively. Wild-type ClyA and its variants were obtained in their completely reduced state, as verified by Ellman's assay[32] and reversed-phase high-performance liquid chromatography (HPLC) (see below), and stored at −20 °C in PBS buffer [20 mM KH_2PO_4/K_2HPO_4 and 150 mM NaCl (pH 7.3)] supplemented with 2 mM DTT.

Recombinant TEV protease was produced as described previously.[33] The N-terminal His_6 tag in variant ClyA CC6/264 was cleaved in cleavage buffer [20 mM Tris-HCl (pH 7.5), 100 mM NaCl, and 2 mM β-mercaptoethanol] at 22 °C for 4 h with initial concentrations of 40 and 2 μM for ClyA CC6/264 and TEV protease, respectively.

Oxidation of Wild-Type ClyA and Its Variants. To generate the oxidized (disulfide-bonded) forms of the variants, proteins (30 μM) were incubated in PBS buffer [20 mM KH_2PO_4/K_2HPO_4 and 150 mM NaCl (pH 7.3)] with 0.5 mM $CuCl_2$ as the catalyst for air oxidations for 4 h at room temperature. The oxidized proteins were then dialyzed against PBS containing 2 mM EDTA and subjected to gel filtration on Superdex 200 in PBS buffer to separate monomers from species with higher molecular masses containing intermolecular disulfide bonds. The absence of free thiols in the purified, oxidized monomers was confirmed by Ellman's assay[32] under denaturing conditions.

Crystallization and Determination of the Structure of ClyA CC6/264. The oxidized ClyA variant CC6/264 (after cleavage of the His_6 tag with TEV protease) was crystallized in its monomeric state. Crystals were grown by the sitting-drop vapor diffusion method at 20 °C. Crystals were obtained at a protein concentration of 2.0−6.5 mg/mL at pH 6.0−8.0 with PEG 3350 as the precipitant. Specifically, the crystal yielding the 2.12 Å structure of CC6/264 Thr2−Val302 grew in a drop consisting of 1.5 μL of a 4.0 mg/mL protein solution in 20 mM Tris-HCl (pH 7.3) and 150 mM NaCl and 1.5 μL of the well solution. The well solution (300 μL) consisted of 100 mM Tris-acetic acid (pH 6.5) and 21% PEG 3350. The crystal yielding the 1.94 Å structure of CC6/264 Cys6−Val302 grew in a drop consisting of 1.5 μL of a 5.6 mg/mL protein solution in 20 mM Tris-HCl (pH 7.3) and 150 mM NaCl and 2.5 μL of the well solution. The well solution consisted of 100 mM Tris-acetic acid (pH 6.7) and 19% (w/v) PEG 3350. In both cases, cryoprotection was performed stepwise in the well solution containing 25% glycerol and crystals were frozen in liquid nitrogen.

Data were collected at the PX beamline at the Paul Scherrer Institut (Villigen, Switzerland) equipped with a Pilatus 6M detector in a liquid nitrogen stream at 100 K. The data were processed using XDS.[34] Molecular replacement using the structure of wild-type ClyA (PDB entry 1QOY) with modeled residues 6, 87, 264, and 285 and structural refinement were performed using the Phenix software package[35] and Coot.[36] Table S1 of the Supporting Information shows an overview of the crystallographic and refinement statistics.

Negative Stain Transmission Electron Microscopy. To trigger oligomerization, ClyA (wt or variants; 5 μM in PBS) was mixed with DDM [final concentration of 0.1% (w/v)] and incubated for 1 h at 22 °C. The samples were adsorbed on glow-discharged 300 mesh carbon-coated copper grids (Quantifoil) and negatively stained with 2 mM uranyl acetate. Images were recorded with a KeenView CCD camera using a FEI Morgagni electron microscope operating at an acceleration voltage of 100 kV.

Circular Dichroism (CD) Spectroscopy. The monomer-to-protomer transition of the ClyA monomer (0.3 mg/mL) in PBS

dx.doi.org/10.1021/bi5007578 | *Biochemistry* 2014, 53, 6357−6369

buffer at 22 °C was initiated by addition of DDM [final concentration of 0.1% (w/v)] and followed via the change in ellipticity at 225 nm with a temperature-controlled J715 CD spectrometer (Jasco). Samples of reduced ClyA additionally contained 2 mM DTT. CD spectra and recorded CD kinetics were corrected for the CD signal contributions of the respective buffers (PBS alone or PBS containing 0.1% DDM and/or 2 mM DTT) and converted to mean residue ellipticity. Kinetic traces were fit according to a consecutive mechanism with two irreversible reactions (A → B → C)[37] according to eq 1

$$f(t) = a e^{-k_1 t} + b\frac{k_1}{k_2 - k_1}(e^{-k_1 t} - e^{-k_2 t}) + c\left[1 + \frac{1}{k_1 - k_2}(k_2 e^{-k_1 t} - k_1 e^{-k_2 t})\right] \quad (1)$$

where a−c are the CD signal intensities of the monomer, the intermediate, and the protomer, respectively, and k_1 and k_2 are the rate constants of the A → B and B → C reactions, respectively.

Kinetics of Hemolysis. The kinetics of horse erythrocyte lysis were measured as described previously.[38] Hemolysis was followed via the decrease in the optical density at 650 nm using a Varian Cary 100 spectrophotometer with a stirred cuvette; 2×10^6 horse erythrocytes/mL yielding an initial optical density (OD) of 0.75 were lysed by ClyA at 37 °C in PBS buffer. The kinetics were evaluated by linearly fitting (i) the pretransition baseline and (ii) the data points in the middle of the lysis reaction between 35 and 75% of the initial optical density. The time of lysis onset was defined as the time point at which the two linear fits intersected, and the maximal lysis velocity was defined as the slope of the linear decrease in optical density between 35 and 75% of the initial cellular density (Figure S4C of the Supporting Information).

Kinetics of Reduction of Oxidized wt ClyA and Its Variants. The natural disulfide bond of wt ClyA and the artificial disulfide bonds in variants CC50/190 and CC6/264 (5 μM each) were reduced by 10 mM DTT in PBS buffer (pH 7.3) at 37 °C. The reduction of kinetically trapped intermediates CC50/190 and CC6/264 was measured under the same conditions, but after preincubation in 0.1% DDM for 30 min. After different incubation times, aliquots of the reaction mixtures were removed and disulfide exchange was quenched by addition of $^1/_7$ volume of 98% formic acid. The samples were then separated via reversed-phase HPLC on an analytical Zorbax SB300 C8 column (Agilent) at a flow rate of 1 mL/min and 30 °C by applying an acetonitrile gradient (from 30 to 80% in 0.1% trifluoroacetic acid), and the peak areas of oxidized and reduced protein were quantified by peak integration (Figure S6 of the Supporting Information). The decrease in the fraction of oxidized protein was fit according to pseudo-first-order kinetics.

Fluorescence Measurements with 8-Anilino-1-naphthalenesulfonic Acid (ANS). ANS is a fluorescent dye that binds noncovalently to lipids and hydrophobic regions of proteins. When ANS binds to a hydrophobic environment, the fluorescence emission shows a blue shift of the emission maximum and a significant increase in intensity.[39] Because of the reversible binding and the strong signal change, ANS fluorescence is well-suited to studying conformational transitions proceeding via partially folded, molten globule-like intermediates.[40,41]

All ANS fluorescence measurements were performed in PBS buffer at 22 °C and were recorded with a temperature-controlled PTI Quantum Master 7 fluorescence spectrometer (excitation wavelength of 370 nm, emission wavelength of 475 nm). The respective ClyA monomer (5 μM, reduced, sample containing 20 mM DTT) was preincubated with ANS (20 μM), and the conformational transition to the protomer was initiated by addition of DDM [final concentration of 0.1% (w/v)]. Oxidized variants CC50/190 and CC6/264 were preincubated with ANS and 0.1% DDM, and the conformational transition was started by addition of DTT (final concentration of 20 mM). Data were fit according to a consecutive mechanism (eq 1). In kinetic experiments that were initiated by addition of DDM, a strong, ClyA-independent increase in ANS fluorescence was observed (interaction between DDM and ANS), which was completed in the dead time of manual mixing (≤2 s) and thus had no influence on the evaluation of the fluorescence kinetics in the time window of 5−4000 s.

The dissociation constant of the complex between ANS and the trapped intermediate of oxidized ClyA CC6/264 and its stoichiometry were determined via fluorescence titration. ANS (20 μM) was incubated with 0.1% DDM and different concentrations (0−28 μM) of ClyA for at least 1 h. The fluorescence at 475 nm of each sample was recorded for 60 s, averaged, and plotted against the respective ClyA:ANS ratio. As the data proved to be inconsistent with a single ANS binding site per ClyA molecule, they were tentatively fit according to a binding equilibrium with multiple, independent ANS binding sites per ClyA with identical affinity according to eq 2

$$S = S_0 + 0.5(S_\infty - S_0)\left[1 + \frac{x + K}{p} - \sqrt{1 + \left(\frac{x + K}{p}\right)^2 - 4\frac{x}{p}}\right] \quad (2)$$

where S is the measured ANS fluorescence, x is the concentration of ClyA, S_0 and S_∞ are the fluorescence signals of free and bound ANS, respectively, K is the apparent dissociation constant (K_D), and p is the apparent number of ANS binding sites per ClyA monomer. The deduced K_D and p values served as only empirical parameters describing the properties of the disulfide-trapped intermediates of $CC50/190_{ox}$ and $CC6/264_{ox}$.

Production of Donor/Acceptor-Labeled Variant CC6/264 and Single-Molecule Förster Resonance Energy Transfer (FRET) Experiments. ClyA variant CC6/264 Q56C E252C was purified under reducing conditions as described above. After removal of DTT, it was labeled with Alexa Fluor 488 C_5-maleimide and Alexa Fluor 594 C_5-maleimide prior to formation of the Cys6−Cys264 disulfide bond, because Cys6 and Cys264 are essentially buried and proved to be much less reactive than Cys56 and Cys252. Specifically, ClyA (20 μM) was first incubated with an equal amount of Alexa Fluor 488 C_5-maleimide in 10 mM KH_2PO_4/K_2HPO_4 (pH 7.4) for 4 h at 22 °C. Subsequently, singly labeled protein was separated from unlabeled and doubly labeled protein by anion exchange chromatography at pH 7.4 and 22 °C using a 1 mL Resource Q column (GE Healthcare) (gradient from 0 to 600 mM NaCl over 20 mL). The singly labeled ClyA species was then incubated with Alexa Fluor 594 C_5-maleimide (1:1 stoichiometry) for 4.5 h at 22 °C and pH 7.4. Immediately after the labeling, Cu^{2+}-catalyzed air oxidation of the C6/C264 thiol pair was performed as described above, and the doubly labeled, oxidized ClyA variant was purified via gel filtration on a Superdex 200 column (GE Healthcare) equilibrated in PBS (pH 7.3). The presence of both labels in the preparation at an approximate 1:1 ratio was verified

dx.doi.org/10.1021/bi5007578 | Biochemistry 2014, 53, 6357−6369

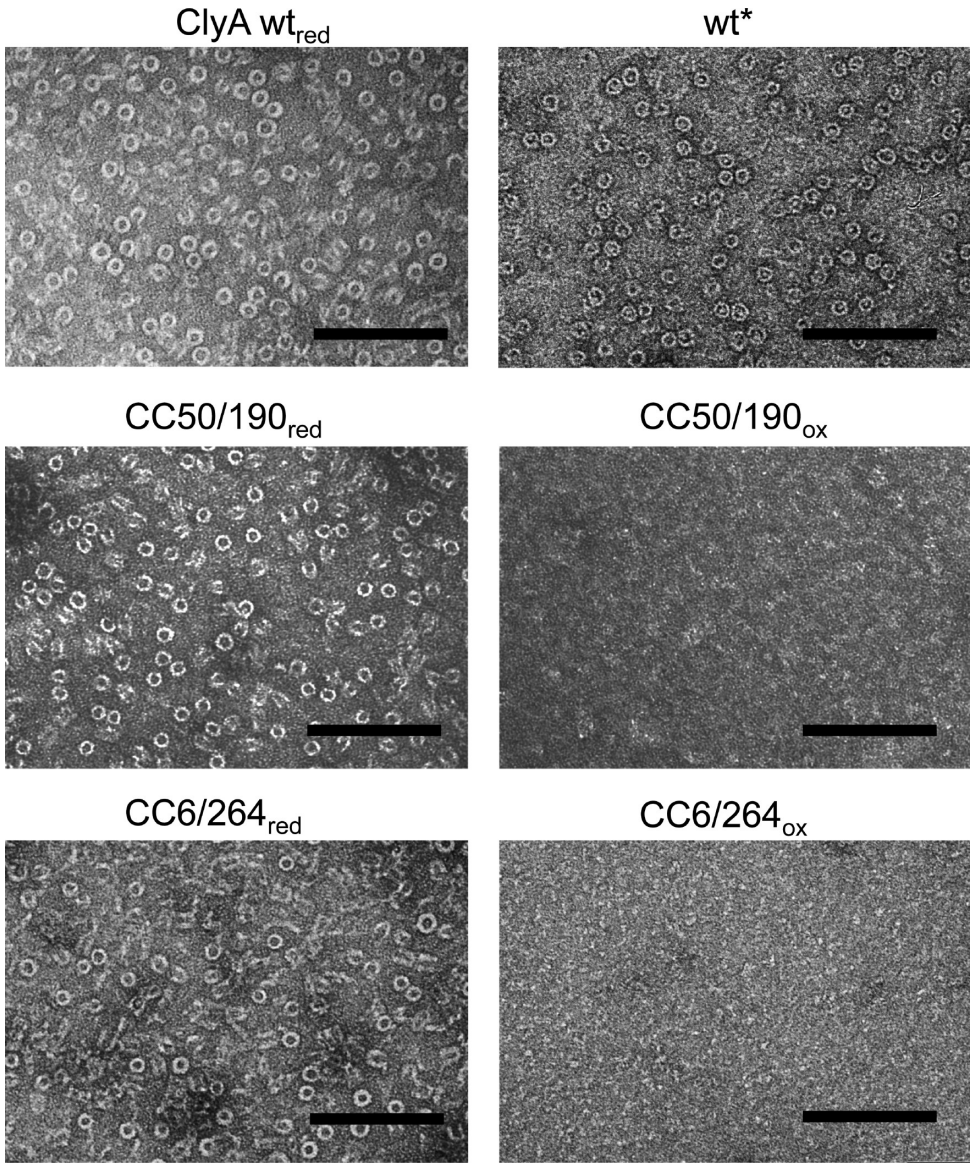

Figure 2. Electron micrographs of negatively stained (2% uranyl acetate) wt ClyA and its variants (monomer concentration of 5 μM) after induction of pore formation with 0.1% DDM at 22 °C and pH 7.3 and incubation for 1 h. Complete oxidation or reduction of the respective ClyA variants prior to addition of DDM was verified by Ellman's assay. The scale bar is 100 nm.

by absorbance spectroscopy (Figure S7A of the Supporting Information) using the following extinction coefficients: 73000 M^{-1} cm^{-1} for Alexa 488 at 495 nm and 92000 M^{-1} cm^{-1} for Alexa 594 at 590 nm. The complete oxidation of the C6/C264 thiol pair in donor/acceptor-labeled variant CC6/264 Q56C E252C was verified by reversed-phase HPLC on a Zorbax 300SB C8 column with a 30 to 80% acetonitrile gradient (Figure S7B of the Supporting Information). Doubly labeled, reduced CC6/264 proved to retain hemolytic activity (Figure S7C of the Supporting Information).

Single-molecule FRET measurements were recorded on a modified Micro Time 200 confocal instrument (PicoQuant) as described previously.[42] To eliminate the contribution of donor-only labeled molecules, pulsed interleaved excitation was used.[43] The donor dye was excited at 485 nm with a diode laser (LDH-D-C-485, PicoQuant) at a power of 100 μW and the acceptor dye with filtered light (z582/15 bandpass filter, Chroma) from a white light continuum source (SC-450-6, Fianium) at a power of 50 μW at 585 nm. All measurements were performed at 22 °C at a protein concentration of 100 pM in 20 mM KH_2PO_4/K_2HPO_4 (pH 7.3) containing 150 mM NaCl and 100 mM DTT in the case of reduced ClyA, in the presence or absence of 0.1% (w/v) DDM. Fluorescence bursts originating from single molecules diffusing through the confocal observation volume were identified and selected from the recorded data as described previously[44] with a threshold of 50 photons per burst. The transfer efficiency histograms were fit with log-normal and Gaussian distributions to determine the mean transfer efficiency.

Accession Numbers of X-ray Structures in the PDB. The coordinates of ClyA CC6/264 (2−303) and CC6/264 (6−303) have been deposited in the PDB as entries 4PHO [CC6/264 (2−303)] and 4PHQ [CC6/264 (6−303)], respectively.

RESULTS

Design of Disulfide-Trapped Variants CC50/190 and CC6/264 and Crystal Structure of Trapped Variant CC6/264. Wild-type (wt) ClyA from *E. coli* is a 303-residue protein with a single cysteine pair (C87 and C285) that can form a

dx.doi.org/10.1021/bi5007578 | *Biochemistry* 2014, 53, 6357−6369

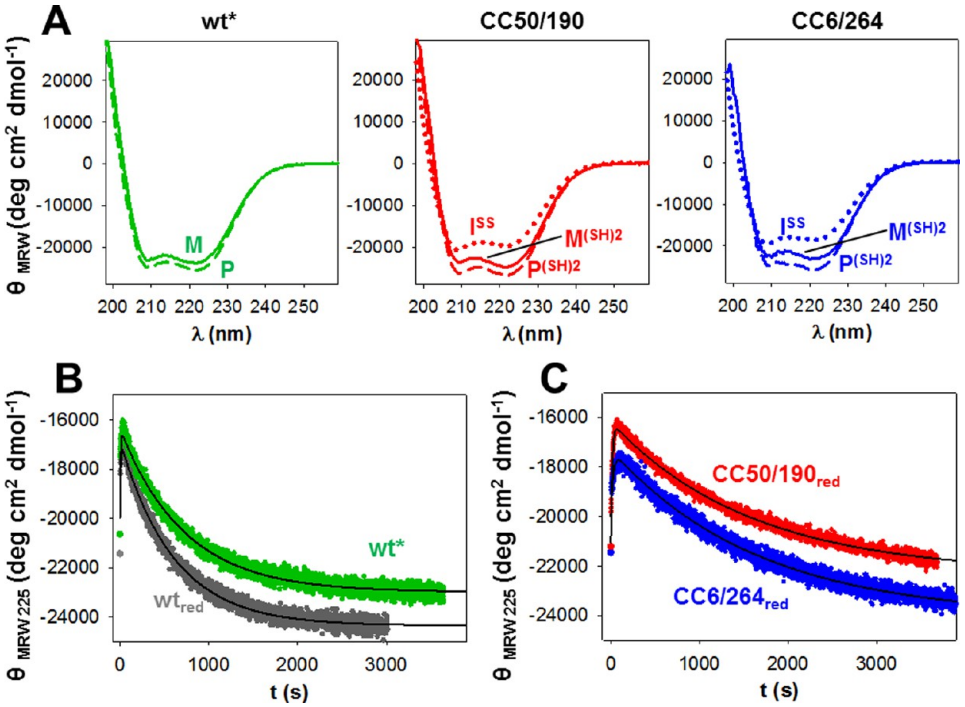

Figure 3. Spectrocopic characterization and kinetics of the monomer-to-protomer transition at 22 °C and pH 7.3 of wt ClyA, wt*, CC50/190, and CC6/264 (8.9 μM each). (A) Far-UV CD spectra of different conformational states of wt* (left), CC50/190 (middle), and CC6/264 (right). Spectra are shown for the soluble monomers in the absence of DDM [M for wt* and $M^{(SH)2}$ for the reduced monomers of CC50/190 and CC6/264 (solid lines)], for the protomers in assembled pores [P for wt* and $P^{(SH)2}$ for the reduced protomers of CC50/190 and CC6/264 (dashed lines)] in the presence of 0.1% DDM, and the disulfide-trapped, DDM-induced intermediates [I^{SS} (dotted lines)] of CC50/190 and CC6/264. (B and C) Kinetics of the conformational transition of wt ClyA and wt* (B) and reduced variants CC50/190 and CC6/264 (C), initiated by addition of 0.1% DDM and followed via the change in the CD signal at 225 nm. Complete reduction of the ClyA variants prior to addition of DDM was verified by Ellman's assay. Data were fit according to two consecutive, irreversible reactions (eq 1, solid black lines). The deduced rate constants are summarized in Table 1.

Table 1. Kinetics of the DDM-Induced Conformational Monomer-to-Protomer Transition, Disulfide Bond Reduction, and Hemolysis Activity at pH 7.3 of the Different ClyA Variants[a]

	wt_{red}	wt*	$CC50/190_{red}$	$CC50/190_{ox}$	$CC6/264_{red}$	$CC6/264_{ox}$
Kinetics of the DDM-Induced Conformational Transition at 22 °C $M \xrightarrow{k_{MI}} I \xrightarrow{k_{IP}} P$						
$k_{DTT+DDM\ 22}$ (M^{-1} s^{-1})[b]	na[f]	na[f]	na[f]	$(2.6 \pm 0.1) \times 10^{-1}$	na[f]	$(3.9 \pm 0.1) \times 10^{-1}$
$k_{MI\ CD}$ (s^{-1})[c]	$(1.5 \pm 0.4) \times 10^{-1}$	$(1.6 \pm 0.3) \times 10^{-1}$	$(8.1 \pm 1.9) \times 10^{-2}$	$(8.5 \pm 0.1) \times 10^{-2}$	$(2.5 \pm 0.3) \times 10^{-2}$	$(1.6 \pm 0.1) \times 10^{-2}$
$k_{MI\ ANS}$ (s^{-1})[d]	$(9.2 \pm 0.1) \times 10^{-2}$	$(1.1 \pm 0.1) \times 10^{-1}$	$(6.4 \pm 0.1) \times 10^{-2}$	$(9.1 \pm 0.1) \times 10^{-2}$	$(2.0 \pm 0.1) \times 10^{-2}$	$(2.1 \pm 0.1) \times 10^{-2}$
$k_{IP\ CD}$ (s^{-1})[c]	$(1.5 \pm 0.1) \times 10^{-3}$	$(1.5 \pm 0.1) \times 10^{-3}$	$(5.5 \pm 0.3) \times 10^{-4}$	na[f]	$(9.4 \pm 0.8) \times 10^{-4}$	na[f]
$k_{IP\ ANS}$ (s^{-1})[d]	$(1.7 \pm 0.1) \times 10^{-3}$	$(1.5 \pm 0.1) \times 10^{-3}$	$(7.8 \pm 0.1) \times 10^{-4}$	na[f]	$(1.5 \pm 0.1) \times 10^{-3}$	na[f]
Specific Hemolytic Activity at 37 °C						
specific activity (mOD s^{-1} nM^{-1})	0.96	0.48	0.70	0	0.16	0
relative activity (% of wt)	100	50	73	0	17	0
Comparison of the Resistance against Reduction by DTT at 37 °C of the Disulfide Bonds of $CC50/190_{ox}$ and $CC6/264_{ox}$ in the Monomer and the I^{SS} State[e]						
$k_{DTT\ 37}$ (M^{-1} s^{-1})[b]	na[f]	na[f]	na[f]	1.6 ± 0.1	na[f]	$(2.4 \pm 0.1) \times 10^{-2}$
$k_{DTT+DDM\ 37}$ (M^{-1} s^{-1})[b]	na[f]	na[f]	na[f]	$(8.6 \pm 0.1) \times 10^{-1}$	na[f]	1.2 ± 0.1

[a]Figure S9 of the Supporting Information shows simulated populations of M, I, and P using k_{MI} and k_{IP} values determined by ANS fluorescence measurements. [b]Measured by acid quenching after different reaction times and HPLC separation of oxidized and reduced ClyA (Figure 6A and Figure S5 of the Supporting Information). [c]Recorded by the change of the CD signal at 225 nm after initiation of the reaction by manual mixing or stopped flow (oxidized variants). [d]Recorded via the change in ANS fluorescence at 475 nm (manual mixing). Rate constants for wt, wt*, and reduced variants refer to the kinetics shown in Figure 6D. Rate constants k_{MI} for $CC50/190_{ox}$ and $CC6/264_{ox}$ were obtained from the experiment shown in Figure 6B. [e]Compare to Figure S5 of the Supporting Information. [f]Not applicable.

disulfide bond. The detergent- and membrane-induced conversion of the monomer to the dodecameric pore complex proved to be independent of the redox state of this cysteine pair.[23] The X-ray structure of the ClyA wt monomer was determined for the reduced form.[21] To eliminate the formation of wrong disulfide bonds in ClyA variants bearing an additional, engineered, disulfide bond, we first generated a cysteine-deficient ClyA variant, termed wt*, in which C87 and C285 were replaced with alanine residues. Like the reduced wild-type protein, wt* proved to be fully assembly competent upon addition of the detergent *n*-dodecyl β-D-maltopyranoside (DDM), as judged by negative stain electron microscopy (Figure 2). In addition, wt*

dx.doi.org/10.1021/bi5007578 | *Biochemistry* 2014, 53, 6357−6369

showed transition and assembly kinetics identical within experimental error to those of the reduced wild type, characterized by rapid formation of an intermediate with less negative ellipticity at 225 nm relative to that of the monomer in the absence of detergent, and a slow, rate-limiting conversion to the protomer with increased negative ellipticity, consistent with the higher α-helix content of the protomer[5] (Figure 3A,B and Table 1). On the basis of these results and the X-ray structure of the reduced ClyA monomer,[21] we engineered two variants of wt*, termed CC50/190 and CC6/264, in which an additional cysteine pair was introduced to trap ClyA at intermediate stages of its DDM-induced monomer-to-protomer transition (see Materials and Methods for details). In variant CC50/190, which was designed by manual modeling in PyMOL,[29] the engineered disulfide between C50 and C190 would fix the ClyA β-tongue to the N-terminus of the structurally conserved helix B and prevent the proposed upward swinging of the β-tongue and its membrane insertion (Figure 1B). The disulfide bond between C6 and C264 in variant CC6/264, which was predicted by "Disulfide by Design",[28] would tie the structurally conserved loop between helices F and G[5] to the N-terminus of helix A and prevent upward swinging and membrane insertion of helix A (Figure 1C). In both CC50/190 and CC6/264, the engineered cysteines are distant in the structure of the protomer (Figure 1B,C), so that disulfide bond formation would completely block protomer formation.

Variants CC50/190 and CC6/264 bearing cleavable, N-terminal hexahistidine tags were produced as soluble monomers (Figure S1 of the Supporting Information) in the cytoplasm of *E. coli*, purified in the presence of the reductant dithiothreitol (DTT), and showed far-UV CD spectra very similar to those of wt* (Figure 3A and Figure S3A,B of the Supporting Information). After removal of DTT by gel filtration, the artificial disulfide bond in both variants was formed quantitatively by Cu^{2+}-catalyzed air oxidation.

The disulfide form of the CC6/264 variant could be crystallized in two different crystal forms after cleavage of the N-terminal His_6 tag: (1) one comprising residues 2−303 (corresponding to wt ClyA in which the N-terminal residue M1 is cleaved) and (2) N-terminally truncated form comprising residues 6−303. CC6/264 (2−303) and CC6/264 (6−303) crystallized in space groups $C222_1$ (three monomers per asymmetric unit) and C2 (four monomers per asymmetric unit), respectively. Their X-ray structures were determined by molecular replacement to resolutions of 2.12 and 1.94 Å, respectively (Table S1 of the Supporting Information). The electron density map of the CC6/264 (2−303) structure shown in Figure S2 of the Supporting Information clearly indicates the presence of the artificial disulfide bond in at least one of three protein chains in the asymmetric unit (chain A). In the case of the CC6/264 (6−303) structure, the electron density shows the presence of the disulfide bond in at least one of four chains in the asymmetric unit (Figure S2 of the Supporting Information). The disulfide bonds in the other chains could either not be verified because of a lack of electron density as a consequence of the flexible N-terminal region (chains A and D; chain C of the 2.12 Å structure) or were not observed because of radiation damage[45] (chain C; chain B of the 2.12 Å structure). Besides changes in the local environment of the artificial disulfide bonds, the 2.12 and 1.94 Å structures of CC6/264 showed no significant deviations from that of the wt ClyA monomer, with α-carbon root-mean-square deviations (rmsds) of 0.9 and 0.8 Å, respectively (Figure S2 of the Supporting Information).

The Engineered Disulfide Bonds Render ClyA Variants CC50/190 and CC6/264 Assembly Incompetent. The disulfide forms of CC50/190 and CC6/264 ($CC50/190_{ox}$ and $CC6/264_{ox}$, respectively) proved to be assembly incompetent upon addition of DDM to the monomers, as evidenced by the absence of pore complexes after prolonged incubation in DDM (Figure 2). However, both variants, CC50/190 and CC6/264, formed intact pore complexes in DDM when the engineered disulfides were reduced by DTT prior to addition of DDM (Figure 2). As observed for wt*, the conformational transition of reduced monomer $M^{(SH)2}$ to assembly competent protomer $P^{(SH)2}$ proceeded via the transient population of an intermediate state $[I^{(SH)2}]$ with less negative ellipticity, followed by the rate-limiting, unimolecular transition to $P^{(SH)2}$ (Figure 3B,C). The only significant difference between wt* and the reduced variants ($CC50/190_{red}$ and $CC6/264_{red}$) was a 2.5- and 1.6-fold slower, rate-limiting reaction to the protomer, respectively (Figure 3B,C and Table 1). Like in the case of the reduced wild type (wt_{red}) and wt*, the rate-limiting reaction of formation of assembly competent protomers coincided with the formation of active pores. Samples were removed from the assembly reaction mixtures of ClyA $CC50/190_{red}$ and $CC6/264_{red}$ when a constant circular dichroism (CD) signal at 225 nm had been reached and analyzed for pore complex formation by electron microscopy. Visual inspection of electron micrographs of $CC50/190_{red}$ and $CC6/264_{red}$ at the end of the CD kinetics revealed amounts of wt-shaped pores similar to those of wt_{red} formed under the same conditions (Figure 2). This is consistent with the model[23] in which the assembly of pore complexes from protomers is fast compared to DDM-induced protomer formation, spectroscopically silent in far-UV CD measurements, and not rate-limiting for pore formation for any of the investigated ClyA variants in the used concentration range (5−10 μM) (cf. Figure 3). The results are consistent with a uniform mechanism of DDM-triggered pore assembly for wt_{red}, wt*, $CC50/190_{red}$, and $CC6/264_{red}$ under the applied experimental conditions according to the following scheme:

$$12M^{(SH)2} \xrightarrow{k_{MI}fast} 12I^{(SH)2} \xrightarrow{k_{IP}slow} 12P^{(SH)2} \xrightarrow{fast} \text{pore complex}$$

We note, however, that these data do not allow us to assess the reversibility of the reaction steps or exclude an off-pathway mechanism for the population of I. Far-UV CD spectra of assembly incompetent variants $CC50/190_{ox}$ and $CC6/264_{ox}$ in the presence of DDM showed that both variants adopted a state with a weaker negative CD signal at 225 nm compared to the reduced monomers $[M^{(SH)2}]$ and the reduced protomers $[P^{(SH)2}]$ (Figure 3A). Notably, the CD signal at 225 nm of this trapped state, which we termed I^{SS}, was comparable to the CD signal of the intermediate observed during formation of $P^{(SH)2}$ in the case of $CC50/190_{red}$ and $CC6/264_{red}$. In addition, the rate of DDM-induced I^{SS} formation (k_{MI} in Table 1) was practically identical to the rate with which intermediate $I^{(SH)2}$ of the respective reduced variant was formed (Table 1). No detailed structural information about I^{SS} and $I^{(SH)2}$ is available, but the results indicate that I^{SS} and $I^{(SH)2}$ are very similar. It thus appears that the engineered disulfide bonds in $CC50/190_{ox}$ and $CC6/264_{ox}$ inhibit DDM-induced protomer formation by preventing the intermediate-to-protomer reaction while leaving the monomer-to-intermediate transition unaffected.

Hemolytic Activity as a Quantitative Measure of the Pore Formation Activity of ClyA Variants. Next, we qualitatively compared the hemolytic activity of the reduced

dx.doi.org/10.1021/bi5007578 | *Biochemistry* 2014, 53, 6357−6369

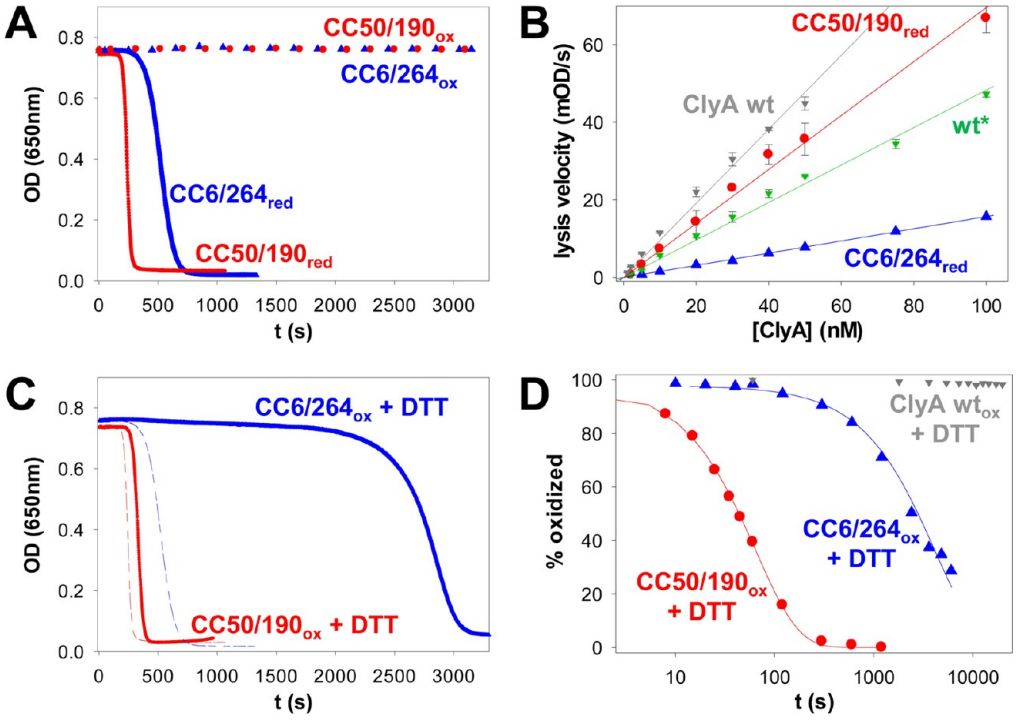

Figure 4. Hemolysis kinetics recorded after mixing of ClyA and its variants with horse erythrocytes (2×10^6 erythrocytes/mL) at 37 °C and pH 7.3. Lysis was recorded via the decrease in the optical density at 650 nm. (A) Hemolysis kinetics recorded for the oxidized and reduced ClyA variants CC50/190 (red) and CC6/264 (blue) (20 nM each, corresponding to a 6×10^6-fold excess of ClyA monomers over erythrocytes). (B) Linear dependence of the maximal lysis velocity on ClyA concentration as a quantitative measure of hemolytic activity. The following parameters were obtained for the different ClyA variants: 0.96 mOD s^{-1} nM^{-1} for wt, 0.48 mOD s^{-1} nM^{-1} for wt*, 0.70 mOD s^{-1} nM^{-1} for CC50/190, and 0.16 mOD s^{-1} nM^{-1} for CC6/264. Error bars show the standard deviation of three independent measurements. (C) Kinetics of activation of oxidized variants CC50/190 (red) and CC6/264 (blue) (20 nM each) by reduction with 10 mM DTT in the presence of horse erythrocytes (reactions were initiated by addition of DTT). The dashed lines show the hemolysis kinetics of the fully reduced variants (cf. panel A). (D) Kinetics of the reduction of the single disulfide bond in oxidized wt ClyA (gray triangles) and oxidized variants CC50/190 (red circles) and CC6/264 (blue triangles) by 200 mM DTT (wt) or 10 mM DTT (variants) at 37 °C and pH 7.3. The reaction was acid-quenched after different times, and the oxidized and reduced species were separated and quantified by reversed-phase HPLC (Figure S6 of the Supporting Information). The disulfide bond of oxidized wt ClyA is resistant to DTT under these conditions, while the engineered disulfides in CC50/190 and CC6/264 are reduced with second-order rate constants of 1.55 ± 0.02 M^{-1} s^{-1} and $(2.41 \pm 0.11) \times 10^{-2}$ M^{-1} s^{-1}, respectively. Solid lines correspond to pseudo-first-order fits.

and oxidized variants CC50/190 and CC6/264 by monitoring the decrease in horse erythrocyte density after addition of the ClyA monomers.[23] In their reduced state, both CC50/190 and CC6/264 showed clear hemolytic activity, with a hemolysis time course similar to that of wt ClyA and wt* (cf. Figure S3C of the Supporting Information).[23] Specifically, the reactions showed an initial lag phase, followed by a fast decrease in cell density and a slow final phase until lysis was completed (Figure 4A). As expected, the disulfide forms of CC50/190 and CC6/264 showed no hemolytic activity, even after long-term incubation with erythrocytes (Figure 4A).

For a quantitative determination of the specific hemolytic activity of the different ClyA variants, we next determined the maximal hemolysis velocity and time of lysis onset based on the hemolysis profiles as a function of the ClyA monomer concentration (see Figure S4C of the Supporting Information). We found that the maximal lysis velocity, defined as the linear decrease in cell density between 65 and 35% of the initial density, correlated linearly with ClyA monomer concentration in the range of 1−100 nM when an initial erythrocyte concentration of 2×10^6 cells/mL was used (Figure 4B and Figure S4A of the Supporting Information). We also observed a nearly linear dependence of the inverse times of lysis onset on ClyA concentration (Figure S4B of the Supporting Information). The results in Figure 4B and Table 1, with the maximal lysis velocity as a measure of ClyA activity, show that wt*, CC50/190_{red}, and CC6/264_{red} still possess 50, 73, and 17% of the specific hemolytic activity (in mOD s^{-1} nM^{-1}) of reduced wt, respectively. The low activity of ClyA variant CC6/264_{red} might not just be the result of a slower conversion to the assembly competent protomer considering that wt* forms the protomer ~2.5 times faster than CC50/190_{red} in DDM (Figure 3 and Table 1) but nevertheless has a lower hemolytic activity (Figure 4B). Therefore, differences in hemolytic activity might also be directly correlated with different specific permeabilities of the assembled pores.

Kinetics of Reductive Activation of CC50/190_{ox} and CC6/264_{ox}. We next investigated the kinetics of activation of the oxidized forms of CC50/190 and CC6/264 by the reductant DTT. Erythrocytes were first incubated with disulfide-trapped variant CC50/190_{ox} or CC6/264_{ox}. Then the reduction of the ClyA variants was started by addition of 10 mM DTT at 37 °C. Figure 4C shows that DTT recovered the pore forming activity of both variants, which completely lysed the erythrocytes after reduction. Compared to experimental data depicted in Figure 4A, where hemolysis was initiated with the fully reduced variants, disulfide-trapped variant CC50/190_{ox} showed a 1.4-fold longer lag time and a 1.4-fold lower apparent lysis velocity after addition of DTT, while CC6/264_{ox} showed a 6.1-fold longer lag time and a 2.6-fold lower lysis velocity under the same conditions (Figure

dx.doi.org/10.1021/bi5007578 | Biochemistry 2014, 53, 6357−6369

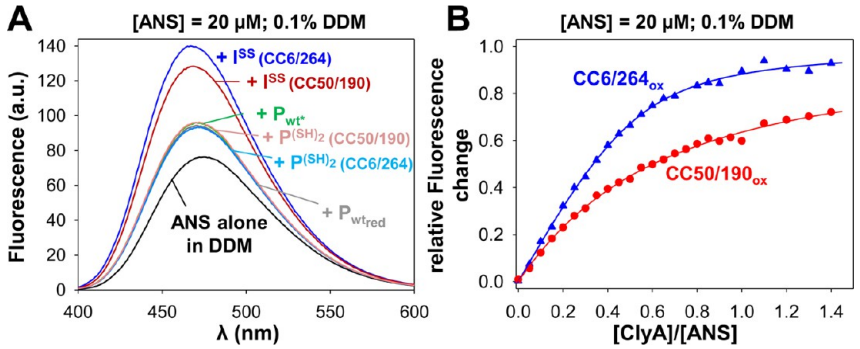

Figure 5. Spectroscopic characterization of the interaction between ANS and the different conformational states of the engineered ClyA variants at pH 7.3 and 22 °C in the presence of 0.1% DDM. (A) Fluorescence spectra in the presence of 0.1% DDM of ANS alone and after addition of protomers and/or pores of reduced wt ClyA ($P_{wt\ red}$) or wt* (P_{wt*}), or the $P^{(SH)2}$ states of reduced CC6/264 or reduced CC50/190. The ANS fluorescence spectra in the presence of the disulfide-trapped, intermediate states (I^{SS}) of ClyA CC6/264 and CC50/190 cause an increase in ANS fluorescence relative to those of all protomers, indicating an increase in surface hydrophobicity in I^{SS} relative to that in $P^{(SH)2}$. All spectra were recorded at pH 7.3 and 22 °C after incubation of the proteins with 0.1% DDM for 2 h, using a constant ANS concentration of 20 μM and protein concentrations of 5 μM (excitation at 370 nm). (B) Fluorescence titration of ANS (20 μM) with the disulfide-trapped variants $CC50/190_{ox}$ and $CC6/264_{ox}$ in the presence of 0.1% DDM. For both variants, the simplest model that is consistent with the data makes the simplifying assumption that I^{SS} possesses several, independent ANS binding sites with identical affinity (eq 2, solid lines). The deduced apparent K_D values and apparent stoichiometries (9.8 ± 3.2 μM and 4.5 ± 3.3 ANS molecules per I^{SS} for CC50/190 and 1.4 ± 0.3 μM and 1.9 ± 0.3 ANS molecules per I^{SS} for CC6/264, respectively) are used here only as empirical parameters describing the properties of the I^{SS} states.

4C). The results show that the reduction of the disulfide-trapped variants by DTT was rate-limiting for cell lysis and indicated that CC50/190 was reduced faster than CC6/264.

For the quantitative characterization of the kinetics of reductive activation of $CC50/190_{ox}$ and $CC6/264_{ox}$, we determined their rates of reduction by DTT in the absence of erythrocytes under the conditions used for the hemolysis reactions (Figure 4D) (37 °C, pH 7.3, and 10 mM DTT). After different incubation times, samples were removed and acid quenched, and mixtures of oxidized and reduced ClyA were separated by reversed-phase HPLC and quantified. Indeed, CC50/190 proved to be reduced 67-fold faster (k_{DTT} = 1.6 M^{-1} s^{-1}) by DTT than CC6/264 (k_{DTT} = 0.024 M^{-1} s^{-1}) (Figure 4D and Table 1). In contrast to those of CC50/190 and CC6/264, the disulfide bond of oxidized wt ClyA was resistant to DTT and could not be reduced even at 20-fold higher DTT concentrations after long-term incubation (Figure 4D).

To obtain information about the accessibility of the engineered disulfides in $CC50/190_{ox}$ and $CC6/264_{ox}$ in a membrane-like environment, we compared their rates of reduction by DTT in the presence and absence of the detergent DDM at 37 °C. Figure S5 of the Supporting Information and Table 1 show that the disulfide in $CC6/264_{ox}$ is 50-fold less protected from reduction in the trapped intermediate I^{SS} than in M^{SS}, while the disulfide of $CC50/190_{ox}$ in its DDM-induced I^{SS} state is reduced with a rate ($k_{DTT+DDM}$) similar to (2-fold lower) that of M^{SS}. In addition, the I^{SS} states of CC50/190 and CC6/264 were reduced with very similar rates (<2-fold difference) at both 22 and 37 °C, indicating that the head domain (disulfide bond in CC50/190) and the tail domain (disulfide bond in CC6/264) region have similar, high surface accessibility in the I^{SS} state of both variants. Their rates of reduction ($k_{DTT+DDM}$) of ~1 M^{-1} s^{-1} at 37 °C (Table 1) are identical within experimental error with a rate of 1.1 M^{-1} s^{-1} for the reduction of completely unfolded wt ClyA in 4 M guanidinium chloride at pH 7.3 and 37 °C (data not shown).

Characterizing the Disulfide-Trapped Intermediates I^{SS} and Their Reductive Activation to Active Pores by the Fluorescent Dye ANS. To further characterize the disulfide-trapped I^{SS} states of CC50/190 and CC6/264 in the presence of DDM, we analyzed their ability to bind the fluorophore 8-anilino-1-naphthalenesulfonic acid (ANS). ANS interacts with exposed hydrophobic regions in proteins, often with high affinity for molten globule-like states, and is an established reagent for monitoring conformational changes in proteins and their surface hydrophobicity.[40,41] Figure 5A shows that binding of ANS to the I^{SS} states of CC50/190 and CC6/264 caused a >2-fold greater increase in ANS fluorescence compared to ANS binding to the protomers of pore complexes formed after reduction with DTT [$P^{(SH)2}$]. In addition, the fluorescence spectra of ANS recorded in the presence of the $P^{(SH)2}$/pore complex states of wt_{red}, wt*, $CC50/190_{red}$, and $CC6/264_{red}$ proved to be identical (Figure 5A). The results indicate that the I^{SS} states of CC50/190 and CC6/264 exhibit higher surface hydrophobicities than their protomers or pore complexes. Titration of ANS with the I^{SS} states of $CC50/190_{ox}$ and $CC6/264_{ox}$ revealed apparent dissociation constants of 9.8 ± 3.2 and 1.4 ± 0.3 μM for I^{SS} states of CC50/190 and CC6/264, respectively (Figure 5B).

We next investigated the kinetics of the reductive activation of the I^{SS} states of CC50/190 and CC6/264 at 22 °C and pH 7.3 in the presence of DDM and their conversion to reduced pore complexes. First, we measured the rates of reduction of the I^{SS} states of both ClyA variants by 20 mM DTT by quenching of the reactions after different times, followed by the RP-HPLC separation of oxidized and reduced protein and peak integration. Figure 6A shows that I^{SS} of CC6/264 was reduced ~2-fold faster than I^{SS} of CC50/190, with rate constants ($k_{DTT+DDM}$) of 0.39 and 0.26 M^{-1} s^{-1}, respectively (see also Table 1). When ANS was included during the reduction of the I^{SS} states, we could observe the transition of the reduced variants to protomers and active pores via the decrease in ANS fluorescence upon protomer formation (Figure 6C). The kinetics of protomer formation showed the lag phase expected for the consecutive reaction mechanism [$I^{SS} \rightarrow I^{(SH)2} \rightarrow P^{(SH)2}$], reproduced the rate constants k_{IP} of the $I^{(SH)2}$ to $P^{(SH)2}$ transitions recorded by CD within a factor of ≤1.6 (Table 1) and confirmed that $CC6/264_{red}$ forms protomers ~2-fold faster than $CC50/190_{red}$ (cf. Figure 3C). Using ANS as a reporter molecule, we could also record the

dx.doi.org/10.1021/bi5007578 | Biochemistry 2014, 53, 6357−6369

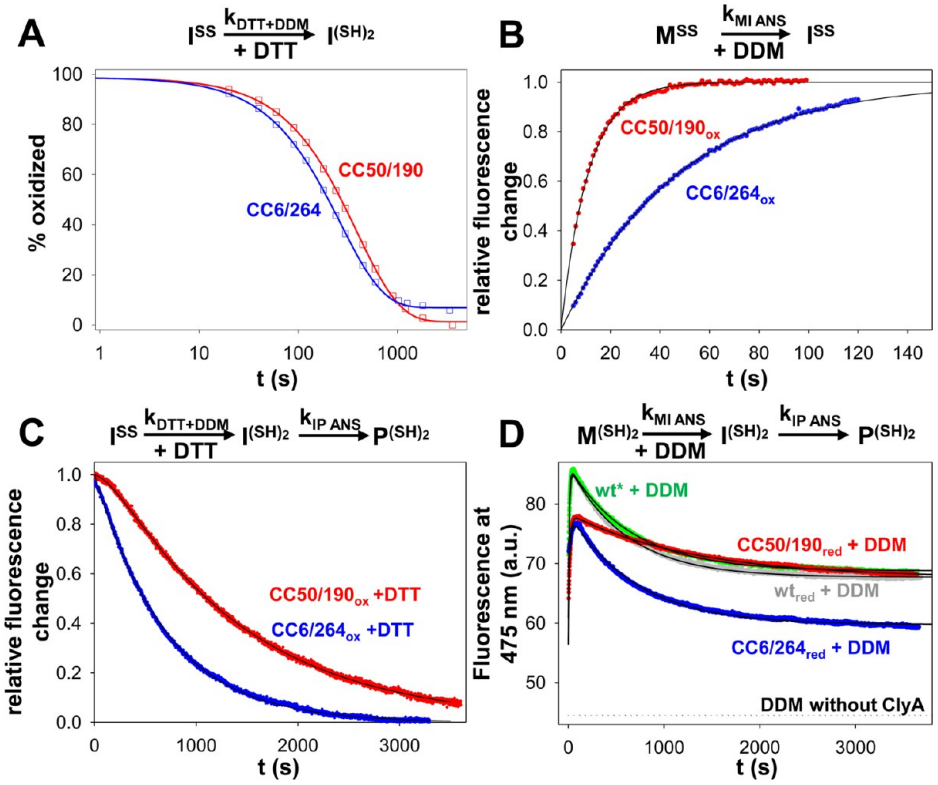

Figure 6. Kinetics of the formation and disappearance of intermediates I^{SS} and $I^{(SH)2}$ in the ClyA monomer-to-protomer transition of ClyA variants CC50/190 and CC6/264 via ANS fluorescence (22 °C and pH 7.3). All measurements were performed with 5 μM ClyA in the presence of 20 μM ANS and 0.1% DDM. (A) Reduction of I^{SS} by DTT (20 mM). The reaction was acid-quenched after different times, and the oxidized and reduced species were separated and quantified by reversed-phase HPLC. Data were fit according to a pseudo-first-order mechanism and normalized (solid lines). (B) Kinetics for formation of I^{SS} from monomers (M^{SS}), initiated by addition of DDM. Data were fit according to a first-order mechanism and normalized (solid lines). (C) Intermediate-to-protomer transition of the disulfide-trapped variants, initiated by addition of 20 mM DTT. The fits according to two consecutive first-order reactions (solid lines) reproduced the independently determined $k_{DTT+DDM\ 22}$ values from panel A (cf. Table 1). Data were normalized assuming that the first step (reduction of I^{SS}) is spectroscopically silent. (D) Monomer-to-protomer transition of the reduced variants, initiated by addition of DDM (0.1%). The fits according to two consecutive first-order reactions (solid lines) reproduced the independently determined k_1 values from panel B (cf. Table 1). Original fluorescence data are shown to indicate the higher fluorescence of ANS bound to $I^{(SH)2}$ of wt and wt* compared to $I^{(SH)2}$ of ClyA CC50/190 and CC6/264. The dashed line indicates the fluorescence of ANS alone after addition of DDM (fluorescence baseline without protein). In panels B and D, a ClyA-independent ANS fluorescence increase upon addition of DDM was completed within the dead time of manual mixing (≤2 s).

kinetics of the DDM-triggered formation of the I^{SS} states of CC50/190 and CC6/264 from their oxidized monomers (M^{SS}) via an increase in ANS fluorescence, which revealed a 5.3-fold faster formation of I^{SS} for $CC50/190_{ox}$ than for $CC6/264_{ox}$ (Figure 6B and Table 1). The reporter dye ANS thus allowed us to monitor the M → I and I → P transition via an initial increase in ANS fluorescence and then a fluorescence intensity decrease, respectively. To confirm this, we recorded the complete M → I → P transition for wt_{red}, wt*, $CC50/190_{red}$, and $CC6/264_{red}$ via ANS fluorescence under the conditions of the reactions followed by far-UV CD (cf. Figure 3C). Figure 6D and Table 1 show that the respective rate constants for the M → I and I → P transitions (k_{MI} and k_{IP}, respectively) agreed very well with those determined by CD kinetics. ANS thus represents a promising, generally applicable spectroscopic probe for conformational transitions of pore-forming toxins.

Single-Molecule FRET Experiments Show that the I^{SS} State of CC6/264 Adopts an Expanded Conformation. To obtain further information about the structural properties of the I^{SS} state, we introduced two additional cysteine residues at positions 56 and 252 into variant CC6/264 for labeling with Alexa Fluor 488 and 594 as the fluorescent donor and acceptor dyes, respectively (residues 56 and 252 are surface-exposed in both the monomer and the protomer). We selected the CC6/264 variant for FRET experiments as its engineered cysteine pair (C6/C264) is more buried in the monomer than that of CC50/190 (cf. Figure 4D), which allowed selective labeling of residues 56 and 252, followed by Cu^{2+}-catalyzed air oxidation of the C6/C264 pair. The Alexa 488/594 donor/acceptor pair has a Förster radius of 5.4 nm.[46] The expected FRET efficiency based on the C_α distances between residues 56 and 252 of 5.50 and 4.45 nm in the monomer and protomer, respectively, is ∼0.46 for the monomer and ∼0.76 for the protomer of CC6/264 (Figure 7A). Figure 7B shows the transfer efficiency histograms and the resulting mean transfer efficiencies (E) recorded for states M^{SS}, $M^{(SH)2}$, I^{SS}, and $P^{(SH)2}$ of donor/acceptor-labeled CC6/264 under equilibrium conditions (pH 7.3, 22 °C). The measured mean transfer efficiencies of M^{SS} and $M^{(SH)2}$ (0.44 and 0.48, respectively) were in the expected range, and the transfer efficiency of $P^{(SH)2}$ (0.70) was also close to the expected value of ∼0.76. For the I^{SS} state, we measured a mean transfer efficiency of 0.15. Assuming an unfolded state and using the distance distribution of a Gaussian chain as an approximation,[42] this transfer efficiency results in a mean-square distance of 11 nm between the label positions. This demonstrates a significant increase in the donor−acceptor distance in I^{SS} compared to that

dx.doi.org/10.1021/bi5007578 | Biochemistry 2014, 53, 6357−6369

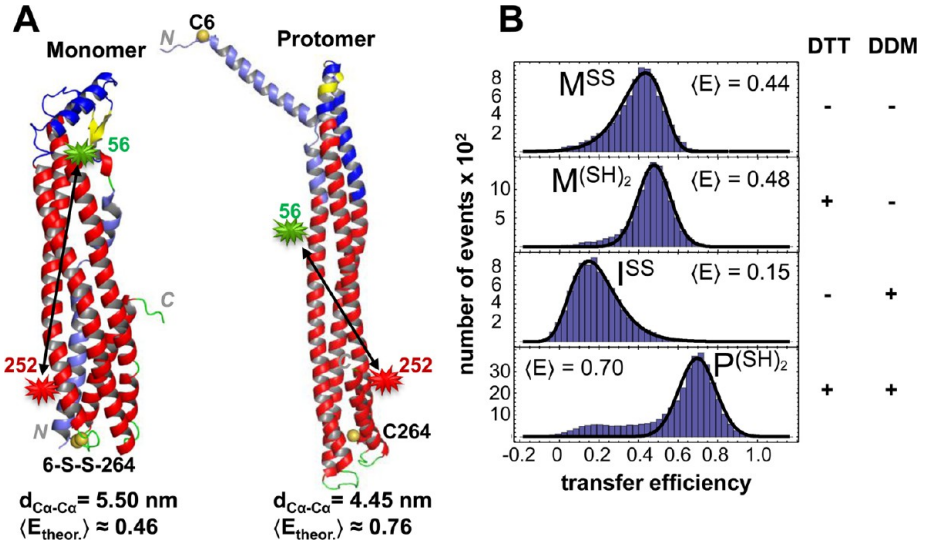

Figure 7. Single-molecule FRET measurements of the different states of ClyA CC6/264 Q56C E252C. (A) Structures of the monomer (PDB entry 1QOY) and protomer (PDB entry 2WCD), with the positions of the fluorescence donor (Alexa 488) at residue 56 (green) and the fluorescence acceptor (Alexa 594) at residue 252 (red), and the approximate FRET efficiencies (E_{theor}) expected for the monomer and protomer, calculated on the basis of the indicated $C_α$−$C_α$ distances (black arrows) between the labeled cysteine residues. (B) Transfer efficiency histograms of ClyA CC6/264 in the presence (+) or absence (−) of DTT and/or DDM as indicated at the right. The indicated values of transfer efficiency result from fitting the histograms with a Gaussian or log-normal distribution (thick black lines) for samples measured in the absence or presence of DTT, respectively. The smaller tailing and reduced peak width in the histogram recorded in the presence of DTT most likely originates from beneficial effects of the thiols of DTT on the photochemical properties of the fluorophores.[48,49]

in the monomer and is indicative of (partial) loss of tertiary structure. This result, together with the preferred binding of I^{SS} to ANS (Figure 5A) and the fact that I^{SS} retains a high content of α-helical secondary structure (Figure 3A), hints at a molten globule-like conformation of I^{SS}.

DISCUSSION

In this study, we have used a novel approach for generating pore-forming toxins with a redox switch. In contrast to previously reported data on redox-regulated α- and β-PFTs with engineered disulfide bonds,[24−27] we have followed a strategy in which disulfide bonds were introduced at different sites into a monomeric PFT that completely block its membrane- or detergent-induced conversion to an assembly competent protomer. For this specific approach, the α-PFT ClyA proved to be an ideal model system, as it is the only known PFT for which a unimolecular reaction of the monomer to an assembly competent protomer is rate-limiting for pore formation, and not a higher-order subunit association reaction to the pore complex.[23] Indeed, the disulfide forms of engineered variants CC50/190 and CC6/264 could not form active pore complexes (cf. Figure 2 and Figure S8 of the Supporting Information) and stayed trapped in a monomeric intermediate state (I^{SS}) showing increased hydrophobicity and decreased secondary structure content under conditions where the reduced forms of the variants formed active pores. The oxidized monomers of variants CC50/190 and CC6/264 were readily reactivated to lytic pore complexes by reduction with DTT, with specific hemolytic activities 1.5-fold higher and 2.9-fold lower than that of wt*, respectively (Table 1). Our observations that kinetic profiles of hemolysis assays can be used to quantify ClyA concentration in the range of 1−100 nM with high accuracy and that maximal lysis velocity correlated linearly with ClyA concentration may prove to be generally applicable for quantifying and comparing specific activities of ClyA variants and even other PFTs.

Besides the use of the disulfide-trapped ClyA variants as dormant lysis factors that can be activated with reducing agents and lyse cells with a defined lag time and lysis velocity, they might also become tools for the elimination of specific cell types in tissues or cell mixtures. Because of the ability of ClyA to retain pore forming activity when it is N- or C-terminally fused to other proteins,[20,47] fusion of disulfide-trapped ClyA variants to cell-type-specific binding proteins could direct ClyA to target cells without affecting other cells, followed by reductant-induced target cell lysis.

The reduced forms of variants CC50/190 and CC6/264 retained the sequential mechanism of detergent-induced pore assembly observed for wt_{red} and wt* and populated a kinetic intermediate with properties reminiscent of a molten globule state. Compared to the respective monomer or protomer, this intermediate showed a lowered α-helical secondary structure content and increased surface hydrophobicity for all ClyA variants investigated. Formation of the kinetic intermediate in the presence of detergent proceeded ∼2 orders of magnitude faster than its conversion to the assembly competent protomer for all variants (Table 1), indicating that formation of the elongated four-helix bundle of the ClyA tail region is rate-limiting in protomer formation.

The reduced kinetic intermediates $I^{(SH)2}$ of CC50/190 and CC6/264 cannot be trapped and correlated directly with the corresponding I^{SS} state under equilibrium conditions. They are, however, transiently populated to more than 92 and 81%, respectively (Figure S9 of the Supporting Information), so that their spectroscopic properties at the time of maximal population can be compared with those of the corresponding I^{SS} states. This analysis revealed that $I^{(SH)2}$ and I^{SS} showed very similar structural features with regard to secondary structure content and surface hydrophobicity for both variants. The most striking similarity between $I^{(SH)2}$ and I^{SS} is their practically identical rate of formation from monomers upon addition of detergent (k_{MI})

dx.doi.org/10.1021/bi5007578 | Biochemistry 2014, 53, 6357−6369

(Table 1). It remains to be shown whether the I^{SS} states are indeed equivalent to $I^{(SH)2}$ formed in the DDM-induced assembly pathway of ClyA, but they may be accessible to crystallization in the presence of detergent and X-ray structure determination. Whether detergent-induced states $I^{(SH)2}$ and I^{SS} correspond to the distinct intermediates in the proposed assembly mechanism of ClyA in the presence of membranes (cf. Figure 1A) remains another open question.

The specific lytic activities of the active ClyA variants differed up to 6-fold (Figure 4B and Table 1), which could result from different rates of membrane insertion of monomers, different rates of protomer formation or protomer assembly, or different specific permeabilities of the respective pore complexes. In contrast, the linear dependencies of lysis rate and the nearly linear dependence of inverse lag times on ClyA concentration (Figure 4B and Figure S4 of the Supporting Information) exclude the higher-order reaction of protomer assembly as a parameter defining hemolytic ClyA activity. Consequently, a common feature of detergent- and membrane-induced ClyA pore formation is a rapid pore assembly reaction after the rate-liming formation of protomers.

■ ASSOCIATED CONTENT

Supporting Information

Supporting figures and tables. This material is available free of charge via the Internet at http://pubs.acs.org.

■ AUTHOR INFORMATION

Corresponding Author

*Department of Biology, Institute of Molecular Biology and Biophysics, HPK E17 Schafmattstrasse 20, CH-8093 Zürich, Switzerland. Phone: +41-446336819. E-mail: rudi@mol.biol.ethz.ch.

Present Address

§M.M.: Dectris Ltd., Neuenhoferstrasse 111, CH-5400 Baden, Switzerland.

Funding

This project was funded by the ETH Zurich, the University of Zurich, and the Swiss National Science Foundation within the framework of the "NCCR Structural Biology" program.

Notes

The authors declare no competing financial interest.

■ ACKNOWLEDGMENTS

We thank Dr. Sebastian Klinge, Dr. Martin Schärer, and Dr. Marc Leibundgut for their support in collecting X-ray diffraction data and structure refinement and Dr. Daniel Nettels for providing single-molecule data analysis software and helpful discussions. We are grateful to Beat Blattmann and Celine Stutz-Ducommun (University of Zurich) for allowing crystal screening at the NCCR crystallization facility in Zurich. We thank Hiang Dreher for providing us with TEV protease. Electron microscopy was performed at the Center for Electron Microscopy ETH Zurich (EMEZ).

■ ABBREVIATIONS

PFT, pore-forming toxin; ClyA, Cytolysin A; ANS, 8-anilino-1-naphthalenesulfonic acid; DTT, dithiothreitol; OMV, outer membrane vesicle; DDM, *n*-dodecyl β-D-maltopyranoside; PDB, Protein Data Bank.

■ REFERENCES

(1) Gouaux, E. (1997) Channel-forming toxins: Tales of transformation. *Curr. Opin. Struct. Biol. 7*, 566−573.

(2) Parker, M. W., and Feil, S. C. (2005) Pore-forming protein toxins: From structure to function. *Prog. Biophys. Mol. Biol. 88*, 91−142.

(3) Choe, S., Bennett, M. J., Fujii, G., Curmi, P. M., Kantardjieff, K. A., Collier, R. J., and Eisenberg, D. (1992) The crystal structure of diphtheria toxin. *Nature 357*, 216−222.

(4) Song, L., Hobaugh, M. R., Shustak, C., Cheley, S., Bayley, H., and Gouaux, J. E. (1996) Structure of staphylococcal α-hemolysin, a heptameric transmembrane pore. *Science 274*, 1859−1866.

(5) Mueller, M., Grauschopf, U., Maier, T., Glockshuber, R., and Ban, N. (2009) The structure of a cytolytic α-helical toxin pore reveals its assembly mechanism. *Nature 459*, 726−730.

(6) De, S., and Olson, R. (2011) Crystal structure of the *Vibrio cholerae* cytolysin heptamer reveals common features among disparate pore-forming toxins. *Proc. Natl. Acad. Sci. U.S.A. 108*, 7385−7390.

(7) Vecsey-Semjen, B., Mollby, R., and van der Goot, F. G. (1996) Partial C-terminal unfolding is required for channel formation by staphylococcal α-toxin. *J. Biol. Chem. 271*, 8655−8660.

(8) Degiacomi, M. T., Iacovache, I., Pernot, L., Chami, M., Kudryashev, M., Stahlberg, H., van der Goot, F. G., and Dal Peraro, M. (2013) Molecular assembly of the aerolysin pore reveals a swirling membrane-insertion mechanism. *Nat. Chem. Biol. 9*, 623−629.

(9) Oscarsson, J., Westermark, M., Lofdahl, S., Olsen, B., Palmgren, H., Mizunoe, Y., Wai, S. N., and Uhlin, B. E. (2002) Characterization of a pore-forming cytotoxin expressed by *Salmonella enterica* serovars typhi and paratyphi A. *Infect. Immun. 70*, 5759−5769.

(10) Ludwig, A., von Rhein, C., Bauer, S., Huttinger, C., and Goebel, W. (2004) Molecular analysis of cytolysin A (ClyA) in pathogenic *Escherichia coli* strains. *J. Bacteriol. 186*, 5311−5320.

(11) del Castillo, F. J., Leal, S. C., Moreno, F., and del Castillo, I. (1997) The *Escherichia coli* K-12 sheA gene encodes a 34-kDa secreted haemolysin. *Mol. Microbiol. 25*, 107−115.

(12) Westermark, M., Oscarsson, J., Mizunoe, Y., Urbonaviciene, J., and Uhlin, B. E. (2000) Silencing and activation of ClyA cytotoxin expression in *Escherichia coli*. *J. Bacteriol. 182*, 6347−6357.

(13) Oscarsson, J., Mizunoe, Y., Uhlin, B. E., and Haydon, D. J. (1996) Induction of haemolytic activity in *Escherichia coli* by the slyA gene product. *Mol. Microbiol. 20*, 191−199.

(14) Ludwig, A., Tengel, C., Bauer, S., Bubert, A., Benz, R., Mollenkopf, H. J., and Goebel, W. (1995) SlyA, a regulatory protein from *Salmonella typhimurium*, induces a haemolytic and pore-forming protein in *Escherichia coli*. *Mol. Gen. Genet. 249*, 474−486.

(15) Oscarsson, J., Mizunoe, Y., Li, L., Lai, X. H., Wieslander, A., and Uhlin, B. E. (1999) Molecular analysis of the cytolytic protein ClyA (SheA) from *Escherichia coli*. *Mol. Microbiol. 32*, 1226−1238.

(16) Lai, X. H., Arencibia, I., Johansson, A., Wai, S. N., Oscarsson, J., Kalfas, S., Sundqvist, K. G., Mizunoe, Y., Sjostedt, A., and Uhlin, B. E. (2000) Cytocidal and apoptotic effects of the ClyA protein from *Escherichia coli* on primary and cultured monocytes and macrophages. *Infect. Immun. 68*, 4363−4367.

(17) Jiang, S. N., Phan, T. X., Nam, T. K., Nguyen, V. H., Kim, H. S., Bom, H. S., Choy, H. E., Hong, Y., and Min, J. J. (2010) Inhibition of tumor growth and metastasis by a combination of *Escherichia coli*-mediated cytolytic therapy and radiotherapy. *Mol. Ther. 18*, 635−642.

(18) Wai, S. N., Lindmark, B., Soderblom, T., Takade, A., Westermark, M., Oscarsson, J., Jass, J., Richter-Dahlfors, A., Mizunoe, Y., and Uhlin, B. E. (2003) Vesicle-mediated export and assembly of pore-forming oligomers of the enterobacterial ClyA cytotoxin. *Cell 115*, 25−35.

(19) Ludwig, A., Volkerink, G., von Rhein, C., Bauer, S., Maier, E., Bergmann, B., Goebel, W., and Benz, R. (2010) Mutations affecting export and activity of cytolysin A from *Escherichia coli*. *J. Bacteriol. 192*, 4001−4011.

(20) Kim, J. Y., Doody, A. M., Chen, D. J., Cremona, G. H., Shuler, M. L., Putnam, D., and DeLisa, M. P. (2008) Engineered bacterial outer membrane vesicles with enhanced functionality. *J. Mol. Biol. 380*, 51−66.

(21) Wallace, A. J., Stillman, T. J., Atkins, A., Jamieson, S. J., Bullough, P. A., Green, J., and Artymiuk, P. J. (2000) *E. coli* hemolysin E (HlyE,

ClyA, SheA): X-ray crystal structure of the toxin and observation of membrane pores by electron microscopy. *Cell 100*, 265−276.
(22) Wai, S. N., Westermark, M., Oscarsson, J., Jass, J., Maier, E., Benz, R., and Uhlin, B. E. (2003) Characterization of dominantly negative mutant ClyA cytotoxin proteins in *Escherichia coli*. *J. Bacteriol. 185*, 5491−5499.
(23) Eifler, N., Vetsch, M., Gregorini, M., Ringler, P., Chami, M., Philippsen, A., Fritz, A., Muller, S. A., Glockshuber, R., Engel, A., and Grauschopf, U. (2006) Cytotoxin ClyA from *Escherichia coli* assembles to a 13-meric pore independent of its redox-state. *EMBO J. 25*, 2652−2661.
(24) Hotze, E. M., Wilson-Kubalek, E. M., Rossjohn, J., Parker, M. W., Johnson, A. E., and Tweten, R. K. (2001) Arresting pore formation of a cholesterol-dependent cytolysin by disulfide trapping synchronizes the insertion of the transmembrane β-sheet from a prepore intermediate. *J. Biol. Chem. 276*, 8261−8268.
(25) Kawate, T., and Gouaux, E. (2003) Arresting and releasing staphylococcal α-hemolysin at intermediate stages of pore formation by engineered disulfide bonds. *Protein Sci. 12*, 997−1006.
(26) Duche, D., Izard, J., Gonzalez-Manas, J. M., Parker, M. W., Crest, M., Chartier, M., and Baty, D. (1996) Membrane topology of the colicin A pore-forming domain analyzed by disulfide bond engineering. *J. Biol. Chem. 271*, 15401−15406.
(27) Kristan, K., Podlesek, Z., Hojnik, V., Gutierrez-Aguirre, I., Guncar, G., Turk, D., Gonzalez-Manas, J. M., Lakey, J. H., Macek, P., and Anderluh, G. (2004) Pore formation by equinatoxin, a eukaryotic pore-forming toxin, requires a flexible N-terminal region and a stable β-sandwich. *J. Biol. Chem. 279*, 46509−46517.
(28) Dombkowski, A. A. (2003) Disulfide by Design: A computational method for the rational design of disulfide bonds in proteins. *Bioinformatics 19*, 1852−1853.
(29) *The PyMOL Molecular Graphics System*, version 1.3r1 (2010) Schrödinger, LLC, Portland, OR.
(30) Kunkel, T. A. (1985) Rapid and efficient site-specific mutagenesis without phenotypic selection. *Proc. Natl. Acad. Sci. U.S.A. 82*, 488−492.
(31) Kapust, R. B., Tozser, J., Fox, J. D., Anderson, D. E., Cherry, S., Copeland, T. D., and Waugh, D. S. (2001) Tobacco etch virus protease: Mechanism of autolysis and rational design of stable mutants with wild-type catalytic proficiency. *Protein Eng. 14*, 993−1000.
(32) Ellman, G. L. (1959) Tissue Sulfhydryl Groups. *Arch. Biochem. Biophys. 82*, 70−77.
(33) Finder, V. H., Vodopivec, I., Nitsch, R. M., and Glockshuber, R. (2010) The recombinant amyloid-β peptide Aβ1−42 aggregates faster and is more neurotoxic than synthetic Aβ1−42. *J. Mol. Biol. 396*, 9−18.
(34) Kabsch, W. (1993) Automatic Processing of Rotation Diffraction Data from Crystals of Initially Unknown Symmetry and Cell Constants. *J. Appl. Crystallogr. 26*, 795−800.
(35) Adams, P. D., Afonine, P. V., Bunkoczi, G., Chen, V. B., Davis, I. W., Echols, N., Headd, J. J., Hung, L. W., Kapral, G. J., Grosse-Kunstleve, R. W., McCoy, A. J., Moriarty, N. W., Oeffner, R., Read, R. J., Richardson, D. C., Richardson, J. S., Terwilliger, T. C., and Zwart, P. H. (2010) PHENIX: A comprehensive Python-based system for macromolecular structure solution. *Acta Crystallogr. D66*, 213−221.
(36) Emsley, P., Lohkamp, B., Scott, W. G., and Cowtan, K. (2010) Features and development of Coot. *Acta Crystallogr. D66*, 486−501.
(37) Crespo, M. D., Puorger, C., Scharer, M. A., Eidam, O., Grutter, M. G., Capitani, G., and Glockshuber, R. (2012) Quality control of disulfide bond formation in pilus subunits by the chaperone FimC. *Nat. Chem. Biol. 8*, 707−713.
(38) Rennie, R. P., Freer, J. H., and Arbuthnott, J. P. (1974) The kinetics of erythrocyte lysis by *Escherichia coli* haemolysin. *J. Med. Microbiol. 7*, 189−195.
(39) Slavik, J. (1982) Anilinonaphthalene sulfonate as a probe of membrane composition and function. *Biochim. Biophys. Acta 694*, 1−25.
(40) Uversky, V. N., Winter, S., and Lober, G. (1996) Use of fluorescence decay times of 8-ANS-protein complexes to study the conformational transitions in proteins which unfold through the molten globule state. *Biophys. Chem. 60*, 79−88.
(41) Poklar, N., Lah, J., Salobir, M., Macek, P., and Vesnaver, G. (1997) pH and temperature-induced molten globule-like denatured states of equinatoxin II: A study by UV-melting, DSC, far- and near-UV CD spectroscopy, and ANS fluorescence. *Biochemistry 36*, 14345−14352.
(42) Hoffmann, A., Kane, A., Nettels, D., Hertzog, D. E., Baumgartel, P., Lengefeld, J., Reichardt, G., Horsley, D. A., Seckler, R., Bakajin, O., and Schuler, B. (2007) Mapping protein collapse with single-molecule fluorescence and kinetic synchrotron radiation circular dichroism spectroscopy. *Proc. Natl. Acad. Sci. U.S.A. 104*, 105−110.
(43) Muller, B. K., Zaychikov, E., Brauchle, C., and Lamb, D. C. (2005) Pulsed interleaved excitation. *Biophys. J. 89*, 3508−3522.
(44) Hofmann, H., Hillger, F., Pfeil, S. H., Hoffmann, A., Streich, D., Haenni, D., Nettels, D., Lipman, E. A., and Schuler, B. (2010) Single-molecule spectroscopy of protein folding in a chaperonin cage. *Proc. Natl. Acad. Sci. U.S.A. 107*, 11793−11798.
(45) Weik, M., Ravelli, R. B. G., Kryger, G., McSweeney, S., Raves, M. L., Harel, M., Gros, P., Silman, I., Kroon, J., and Sussman, J. L. (2000) Specific chemical and structural damage to proteins produced by synchrotron radiation. *Proc. Natl. Acad. Sci. U.S.A. 97*, 623−628.
(46) Schuler, B., Lipman, E. A., and Eaton, W. A. (2002) Probing the free-energy surface for protein folding with single-molecule fluorescence spectroscopy. *Nature 419*, 743−747.
(47) Soskine, M., Biesemans, A., Moeyaert, B., Cheley, S., Bayley, H., and Maglia, G. (2012) An engineered ClyA nanopore detects folded target proteins by selective external association and pore entry. *Nano Lett. 12*, 4895−4900.
(48) Campos, L. A., Liu, J., Wang, X., Ramanathan, R., English, D. S., and Munoz, V. (2011) A photoprotection strategy for microsecond-resolution single-molecule fluorescence spectroscopy. *Nat. Methods 8*, 143−146.
(49) Rasnik, I., McKinney, S. A., and Ha, T. (2006) Nonblinking and long-lasting single-molecule fluorescence imaging. *Nat. Methods 3*, 891−893.